Monatshefte für Chemie 128, 785–793 (1997)

Monatshefte für Chemie
Chemical Monthly

Printed in Austria

Chiroptical Properties and Absolute Configurations of the Hypericin Chromophore Propeller Enantiomers

R. Altmann, C. Etzlstorfer, and **H. Falk***

Institut für Chemie, Johannes Kepler Universität, A-4040 Linz, Austria

Summary. The diastereomeric *mono-* and *bis-ω*-appended (*R*)-menthyl hypericin derivatives were studied by means of absorption spectroscopy, circular dichroism measurements, application of the C_2 rule, and semiempirical calculations. This allowed us to assign the absolute configuration (*P*) to the inherently chiral phenanthroperylene quinone chromophore of hypericin, the *bay*-hypericinate ion, and the 1,6-dioxo-tautomer displaying a negative *Cotton* effect of their long wavelength absorption band. From these results and according to the positive chiroptical sign of their long wavelength bands, the absolute configuration (*M*) could be assigned to the stentorin chromophore in the native pigments.

Keywords. *ω*-Menthyl hypericin derivatives; Circular dichroism; Absolute configuration; C_2 rule; Semiempirical calculations.

Chiroptische Eigenschaften und Absolutkonfiguration der Propellerenantiomeren des Hypericinchromophors

Zusammenfassung. Die diastereomeren *mono-* und *bis-ω*-substituierten (*R*)-Menthyl-hypericinderivative wurden mit Hilfe der Absorptionsspektroskopie, von Circulardichroismusmessungen, der Anwendung der C_2-Regel und semiempirischer Rechnungen untersucht. Dies erlaubte die Zuordnung der absoluten Konfiguration (*P*) für den inhärent chiralen Phenanthroperylenchinon-Chromophor von Hypericin, das *bay*-Hypericination und das 1,6-Dioxotautomer, die einen negativen *Cotton*-Effekt ihrer langwelligen Absorptionsbande aufweisen. Auf der Basis dieser Ergebnisse und aufgrund des positiven chiroptischen Signals seiner langwelligen Absorptionsbande wurde dem Stentorinchromophor in den nativen Pigmenten die absolute Konfiguration (*M*) zugeordnet.

Introduction

Due to a C_2 propeller geometry, which has been established by X-ray crystallography [1, 2], *ab initio* [3], and force field calculations [1, 4], hypericin (**1**), its *bay*-phenolate $\mathbf{1}^-$, and its 1,6-tautomer $\mathbf{1}'$ are chiral. Therefore, they should occur as racemic mixtures of their respective enantiomers. Although the heteroassociate between $\mathbf{1}^-$ and human serum albumin has been shown to display a CD spectrum [5], the fundamental chiroptical properties of the hypericin or hypericinate chromophore could not be advanced so far. This has to be blamed on the ambiguity

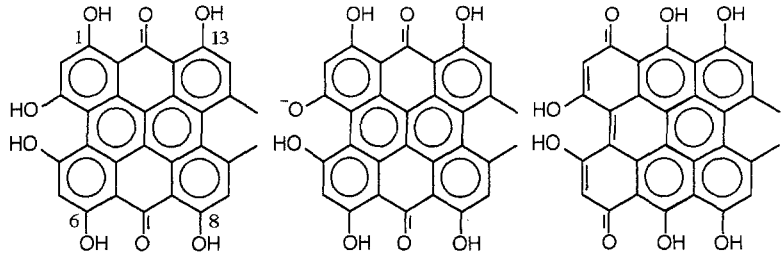

1 1⁻ 1'

that the observed chiroptical signal could either be due to a partial kinetic resolution of one hypericin enantiomer or to a diastereotopic interaction with the protein environment causing an asymmetrical optical induction upon the still racemic chromophore mixture of the associate.

The key to contribute to this problem has been recently made available by the preparation and separation of the two diastereomeric ω-(*R*)-menthyl substituted hypericin diastereomers (*R,P*)-**2**/(*R,M*)-**2** and (*R,R,P*)-**3**/(*R,R,M*)-**3** [6]. In the present report, their chiroptical properties will be investigated to provide this knowledge fundamental to the stereochemistry of hypericin and phenanthroperylene quinones in general.

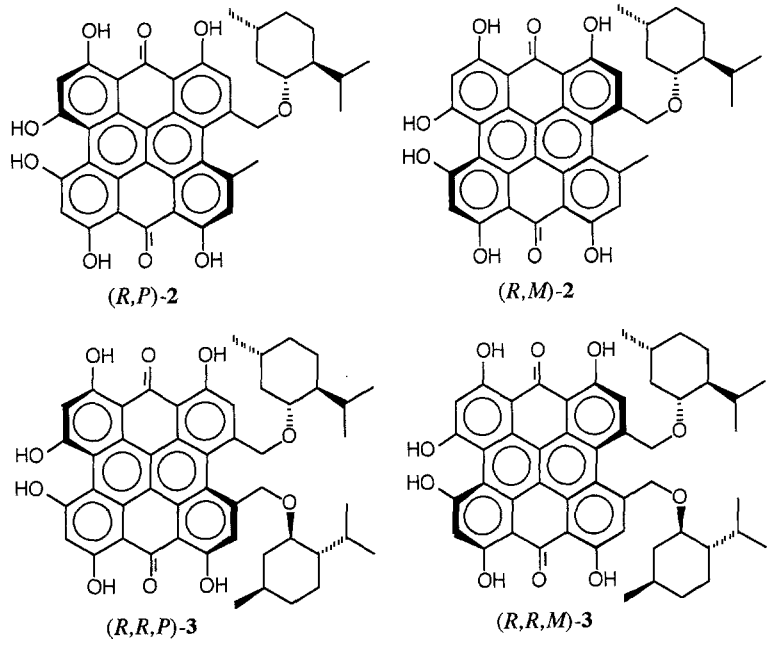

(*R,P*)-**2** (*R,M*)-**2**

(*R,R,P*)-**3** (*R,R,M*)-**3**

Results and Discussion

The general features of the CD spectra of the diastereomers of **2** and **3** are illustrated in Fig. 1 on the example of the CD curves of $\mathbf{2a}^-$ and $\mathbf{2b}^-$, which are shown together with their absorption spectrum. It should be noted that – according to the spectral features of the absorption spectrum of Fig. 1 – the derivatives **2** and

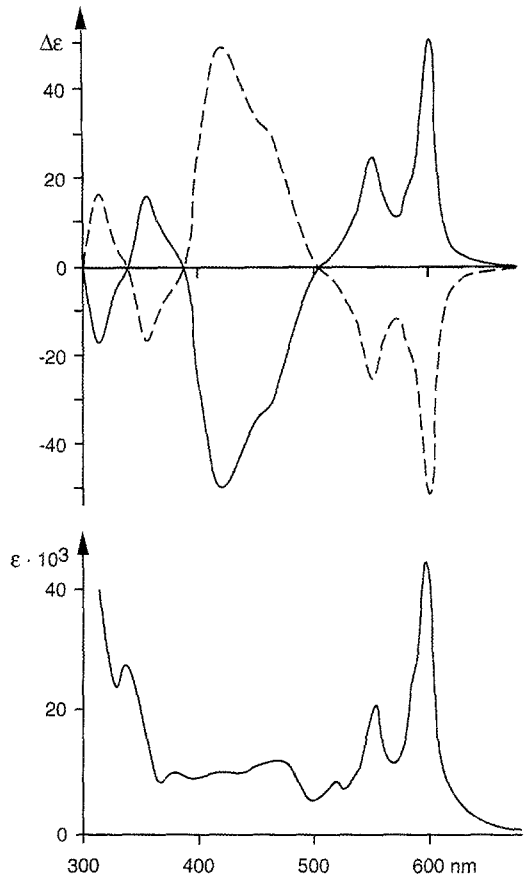

Fig. 1. Circular dichroism spectra of $\mathbf{2a}^-$ (- - -) and $\mathbf{2b}^-$ (—) together with the superimposable UV-Vis spectra of $\mathbf{2a}^-$ and $\mathbf{2b}^-$ dissolved in ethanol (20°C, $c = 3.10^{-6}$ mol/l)

3 are in the ionized states $\mathbf{2}^-$ and $\mathbf{3}^-$ (see also Refs. [6, 7]). The data of $\mathbf{3a}^-$ and $\mathbf{3b}^-$ were found to be superimposable on those presented in Fig. 1. However, acidification of the solution to provoke the non dissociated diastereomeric species **2** and **3** [6], and dissolving the diastereomers of **2** and **3** in tetrahydrofuran, which is known to switch the tautomeric equilibrium in favor of the 1,6-dioxo tautomers **2′** and **3′** [5], did not change the general appearance of these chiroptical properties besides characteristic wavelength shifts and marginal intensity changes (see Experimental). The chiroptical signal wavelengths correlated with those of the absorptions in all cases. The CD curves of the chromatographically faster moving diastereomers **2a** and **3a** (as well as $\mathbf{2a}^-$, **2a′**, *etc.*) exhibited a negative long wavelength CD band system, and they were found to be mirror images of those of their respective diastereomers **2b** and **3b**. This phenomenon immediately pointed to the origin of the chiroptical properties of these compounds. Thus, the mirror image CD curve shapes of the diastereomeric compounds together with the fact that *mono-* and *bis-ω-(R)*-menthyl substitution produced superimposable chiroptical signals related the optical activity exclusively to the inherently chiral phenanthroperylene quinone chromophore. Accordingly, the chiral optical induction of the *(R)*-menthyl moieties upon the hypericin(ate) chromophore was found to be negligible.

At this point it should be mentioned that recently the equilibrium between the diastereomers of **2** and **3** has been investigated, and it has been found that the chromatographically faster moving diastereomers **2a** and **3a** are slightly more stable than their diasteromers **2b** and **3b**. The same holds for their phenolates $\mathbf{2a}^-$ and $\mathbf{3a}^-$ as well as for their respective 1,6-dioxo-tautomers **2a′** and **3a′** [6]. These relative stabilities correlate nicely with the CD data of the equilibrium mixtures, which were found to exhibit long wavelength chiroptical signals with negative signs and appropriate intensities.

The chiroptical data of $\mathbf{2}^-$ and $\mathbf{3}^-$ could now be compared with those which have been observed for $\mathbf{1}^-$ associated with human serum albumin [5]. Thus, it could be established that the preferred *bay*-hypericinate conformer in this heteroassociate had the same configuration as the diastereomers $\mathbf{2b}^-$ and $\mathbf{3b}^-$. Moreover, from the intrinsic chiroptical properties of the hypericinate chromophore and a $\Delta\varepsilon_{600} = +19$ observed for the hypericinate-albumin associate [5] it was concluded that a partial resolution of the *bay*-hypericinate ($\mathbf{1}^-$) had taken place, characterized by a 69:31 distribution of the two hypericinate propeller conformers. This result was in agreement with that derived from a hole burning study of this protein complex in external fields, where it was concluded that if a partial resolution of the two hypericinate propeller conformers had taken place, it had resulted in a mixture not deviating too far from the racemate [8].

The origin of the chiroptical effects and their correlation with the absolute configuration and geometry of the hypericin species propeller conformers could be advanced in principle on two paths – one applying an empirical rule, the other one performing appropriate semiempirical calculations of the various electrical and magnetic transition moments and thus of the optical activity of this system.

The symmetry of the hypericinate ($\mathbf{1}^-$), the 1,6-dioxo-tautomer (**1′**), and, in particular, that of the hypericin (**1**) chromophore is C_2 [1–4]. Thus, the so called C_2 rule of *Wagnière* [9] should be applicable in principle. This rule states that a *transition of symmetry* A in a *right handed* (≡ (*P*)-configured) C_2 symmetrical chromophore will exhibit a *Cotton* effect with *negative sign*; transitions of B symmetry will lead to a positive sign (Fig. 2).

For a successful application of the C_2 rule it was first of all necessary to acquire information about the transition symmetries of the long wavelength absorption bands (which relate to the absorption band polarizations) of hypericin, the hypericinate ion, and the 1,6-dioxo-tautomer. Fortunately, a recent study dealing with polarized absorption spectroscopy and semiempirical calculations of a hypericin derivative appended with long aliphatic chains at the methyl groups and dissolved in a stretched polymer has shown that the long wavelength absorption vibrational band system between 500 and 600 nm of the *bay*-phenolate form is polarized parallel to the C_2 symmetry axis of the molecule (*i.e.*, it is of A symmetry), whereas the two absorption bands between 400 and 500 nm are polarized perpendicular to this axis (*i.e.*, they are of B symmetry) [7]. These polarizations have been in accordance with those derived from semiempirical (PPP) calculations of the phenolate species. Such calculations also have shown that the undissociated form as well as the 1,6-tautomer displayed the same polarization patterns.

As a consequence, application of the C_2 rule (long wavelength transition ⇒ symmetry A ⇒ negative sign ⇒ (*P*)-configuration) led to the assignment of the

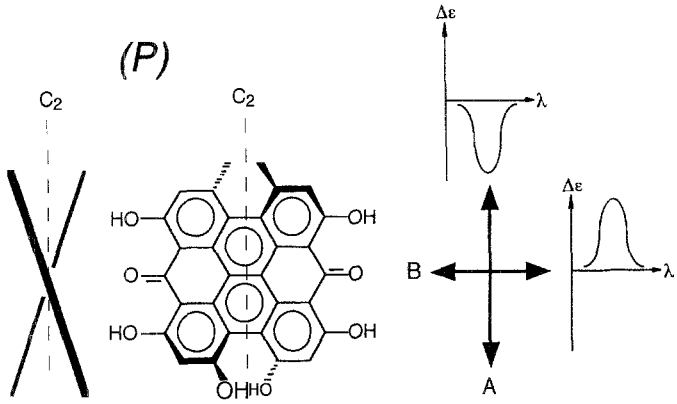

Fig. 2. The C_2 rule as applied to the hypericin chromophore

absolute configuration (*P*) to **2a**, **2a**$^-$, and **2a**′ as well as to **3a**, **3a**$^-$, and **3a**′, whereas **2b**, **2b**$^-$, **2b**′ and **3b**, **3b**$^-$, **3b**′ were assigned the mirror image (*M*)-configuration. This is illustrated in Figs. 3 and 4 with molecular models of the diastereomers **a** and **b** of **2** and **3**, whose geometry was calculated by means of the AM1 method [10]. It should be stressed that these assignments of the absolute configurations of the helical parts of the molecules were also found to be in accordance with the experimental relative thermodynamic stabilities of the respective diastereomers and those calculated by means of the AM1 method.

As can be seen from an inspection of the diastereomers of **2** and **3** in Figs. 2 and 3, the rather small energy difference (the (*P*)-helical diastereomer was found to be stabilized by 3.5 kJ/mol in the case of **2** and by 3.4 kJ/mol in the case of **3**) between the two diastereomers is obviously due to the slightly different orientations of the menthyl moieties. It should be stressed that the energy hypersurfaces of these systems proved to be rather rich in closely spaced energy minima. Nevertheless, the general conformational situation of the menthyl moieties with respect to the hypericin chromophore as described by the semiempirical calculations illustrated in Figs. 3 and 4 could be corroborated using two dimensional NOESY ^{1}H NMR spectroscopy. One of the two CH_2O protons of **2a**$^-$ and **2b**$^-$ displayed more intensive NOE correlations to both the 11-methyl group and the aromatic CH-12 protons, whereas the other one exhibited much lower correlation intensities to these two centers. Additional NOE correlations, *e.g.* between hypericin protons and those of the menthyl moiety, could not be observed indicating ample spatial separation between these two subsystems. Distance measurements on the conformational models of **2a** and **2b** (Fig. 2) showed that in all cases one of the CH_2O protons was placed somewhat closer to both indicator groups, whereas the other one was located further away. Moreover, distance between the hypericin and menthyl protons were found to measure more than 5 Å and thus could not be expected to produce significant NOE correlations.

To proceed beyond the applications of a rule, the optical and chiroptical properties of the hypericin chromophore were also calculated by means of the semiempirical ARGUS method [12]. The results are illustrated in Fig. 5. Comparison of these data with Fig. 1 revealed that – since the parameters of the applied method were not optimized for calculations in this group of compounds –

Fig. 3. Ball & Stick [11] wire frame models of the diastereomers (*R,M*)-**2b** and (*R,P*)-**2a** as calculated by means of the AM1 method

Fig. 4. Ball & Stick [11] wire frame models of the diastereomers (*R,R,M*)-**3b** and (*R,R,P*)-**3a** as calculated by means of the AM1 method

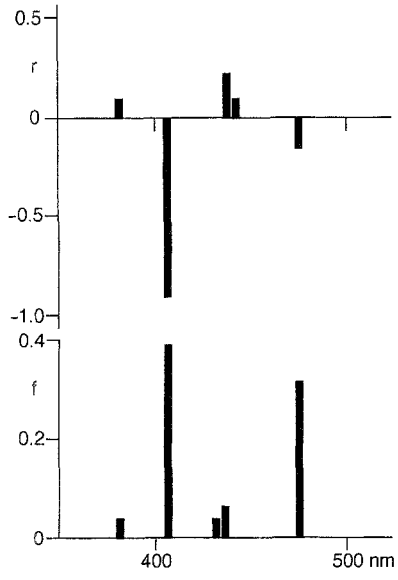

Fig. 5. Calculated circular dichroism and absorption spectra of the (*P*)-configured hypericin chromophore as calculated by means of the ARGUS method [12]

the various transition energies were systematically shifted to shorter wavelengths. To calculate transition energies of such quinones in a quantitative manner, extensive parameter adaption would be necessary as found in the case of the PPP method [7].

Nevertheless, from the calculations shown in Fig. 5 it could be concluded that the order of the absorption bands and their polarization and relative intensities were similar to those found experimentally. Moreover, the signs of the chiroptical properties proved to be identical with those derived for the hypericin (*P*)-configured chromophore by application of the C_2 rule, thus corroborating its absolute configuration. In order to account for the menthyl residues of **2** and **3**, the chiroptical properties of the diastereomers of **2** were also calculated. They were found to be virtually superimposable on the results calculated for **1**, verifying the results obtained above, namely that the chiral appended moieties of **2** and **3** contributed only negligibly to the chiroptical properties of the fundamental hypericin chromophore.

It might be added that since the chromophore of stentorin proteins has the same symmetry (C_2) as hypericin [13], the absolute configuration (*M*) of the stentorin chromophore in the native pigments might be assigned according to the positive chiroptical sign obtained for the long wavelength band [14].

Experimental

The diastereomeric pairs **2a/2b** and **3a/3b** (with diastereomers **a** as the chromatographically faster moving ones and displaying a negative long wavelength circular dichroism band) were prepared and separated as recently reported [6]. The UV/Vis, fluorescence, and circular dichroism measurements were performed on Hitachi-U-3210, Hitachi-F-4010, and ISA-CD-Mark-V instruments at 20°C using ethanol (spectroscopic grade, Merck), ethanol + N,N-diisopropyl-N-ethyl-amine, ethanol + trifluoroacetic acid, and tetrahydrofuran + trifluoroacetic acid as the solvents and sample cells of 0.1–10 cm length. As fluorescence standard the quantum yield of 0.69 of Rhodamine B was

employed. Semiempirical calculations were performed by means of the MOPAC and ARGUS program packages [10, 12] on the CONVEX C3440. For the latter, configuration interaction of 32 out of 92 levels for hypericin were taken into account. The input geometries were assembled from X-ray data on the hypericinate ion [1, 2] and (*R*)-(–)-menthol [15]. ^{1}H NOESY NMR spectra were run using standard conditions in acetone-d_6 on a Bruker DPX-200 instrument.

2a: CD (ethanol + trifluoroacetic acid, $pH \approx 0$, $c = 3 \cdot 10^{-6}$ mol/l): $\lambda_{max} = 578$ (−42), 537 (−27), 456 (+42), 425 (+47), 353 (−21), 322 (+21), nm ($\Delta\varepsilon$).

2b: CD (ethanol + trifluoroacetic acid, $pH \approx 0$, $c = 3 \cdot 10^{-6}$ mol/l): $\lambda_{max} = 578$ (+42), 537 (+27), 456 (−42), 425 (−47), 353 (+21), 322 (−21) nm ($\Delta\epsilon$).

2a/2b: UV/Vis (ethanol + trifluoroacetic acid, $pH \approx 0$, $c = 3 \cdot 10^{-6}$ mol/l): $\lambda_{max} = 582$ (33300), 541 (16900), 504 (6000), 455 (17100), 432 (12500), 327 (23100) nm (ϵ); fluorescence (ethanol + trifluoroacetic acid, $pH \approx 0$, $c = 3 \cdot 10^{-6}$mol/l): $\lambda_{em} = 588$ (1), 634 (0.34) nm (relative intensity), $\Phi_f = 0.20$.

2a$^-$: CD (ethanol + N,N-diisopropyl-N-ethyl-amine, $c = 3 \cdot 10^{-6}$ mol/l): $\lambda_{max} = 589$ (−48), 545 (−26), 475 (+37), 430 (+53), 357 (−17), 318 (+17) nm ($\Delta\varepsilon$); NOESY: H-12 (7.57) ↔ HC*H*-O (5.24), H-12 (7.57) ↔ *H*CH-O (4.85, lower intensity), H-9 (7.46) ↔ CH_3 (2.75), HC*H*-O (5.24) ↔ CH_3 (2.75), *H*CH-O (4.85) ↔ CH_3 (2.75, lower intensity) (ppm).

2b$^-$: CD (ethanol + N,N-diisopropyl-N-ethyl-amine, $c = 3 \cdot 10^{-6}$ mol/l): $\lambda_{max} = 589$ (+48), 545 (+26), 475 (−37), 430 (−53), 357 (+17), 318 (−17) nm ($\Delta\varepsilon$); NOESY: H-12 (7.58) ↔ HC*H*-O (5.04), H-12 (7.58) ↔ *H*CH-O (4.91, lower intensity), H-9 (7.46) ↔ CH_3 (2.70), HC*H*-O (5.04) ↔ CH_3 (2.70), *H*CH-O (4.91) ↔ CH_3 (2.70, lower intensity) (ppm).

2a$^-$**/2b**$^-$: UV/Vis (ethanol + N,N-diisopropyl-N-ethyl-amine, $c = 3 \cdot 10^{-6}$ mol/l): $\lambda_{max} = 592$ (43040), 549 (20140), 511 (7070), 478 (10990), 383 (10420), 329 (26000), 286 (344 20) nm (ε); fluorescence (ethanol + N,N-diisopropyl-N-ethyl-amine, $c = 3 \cdot 10^{-6}$ mol/l): $\lambda_{em} = 600$ (1), 648 (0.3) nm (relative intensity), $\Phi_f = 0.19$.

2a′: CD (tetrahydrofuran + trifluoroacetic acid; c from $3 \cdot 10^{-3}$ to $3 \cdot 10^{-6}$ mol/l): $\lambda_{max} = 578$ (−47), 539 (−23), 457 (+43), 413 (+47), 357 (−14) nm ($\Delta\varepsilon$).

2b′: CD (tetrahydrofuran + trifluoroacetic acid; c from $3 \cdot 10^{-3}$ to $3 \cdot 10^{-6}$ mol/l): $\lambda_{max} = 578$ (+47), 539 (+23), 457 (−43), 413 (−47), 357 (+14) nm ($\Delta\varepsilon$).

2a′/2b′: UV/Vis (tetrahydrofuran + trifluoroacetic acid, $c = 3 \cdot 10^{-5}$ mol/l): $\lambda_{max} = 582$ (32000), 541 (16400), 504 (5800), 455 (16400), 432 (12100), 327 (22500), 286 (34420) nm (ε); fluorescence (tetrahydrofuran + trifluoroacetic acid, $c = 3 \cdot 10^{-6}$ mol/l): $\lambda_{em} = 589$ (1), 636 (0.28) nm (relative intensity), $\Phi_f = 0.21$.

3a: CD (ethanol + trifluoroacetic acid, $pH \approx 0$, $c = 3 \cdot 10^{-6}$ mol/l): $\lambda_{max} = 578$ (−42), 537 (−27), 456 (+42), 425 (+47), 353 (−21), 322 (+21) nm ($\Delta\varepsilon$).

3b: CD (ethanol + trifluoroacetic acid, $pH \approx 0$, $c = 3 \cdot 10^{-6}$ mol/l): $\lambda_{max} = 578$ (+42), 537 (+27), 456 (−42), 425 (−47), 353 (+21), 322 (−21) nm ($\Delta\varepsilon$).

3a/3b: UV/Vis (ethanol + trifluoroacetic acid, $pH \approx 0$, $c = 3 \cdot 10^{-6}$ mol/l): $\lambda_{max} = 583$ (31000), 541 (15800), 504 (5600), 455 (16100), 432 (11600), 327 (21500) nm (ε); fluorescence (ethanol + trifluoroacetic acid, $pH \approx 0$, $c = 3 \cdot 10^{-6}$ mol/l): $\lambda_{em} = 589$ (1), 635 (0.34) nm (relative intensity), $\Phi_f = 0.18$.

3a$^-$: CD (ethanol + N,N-diisopropyl-N-ethyl-amine, $c = 3 \cdot 10^{-6}$ mol/l): $\lambda_{max} = 589$ (−48), 545 (−26), 475 (+37), 430 (+53), 357 (−17), 318 (+17) nm ($\Delta\varepsilon$).

3b$^-$: CD (ethanol + N,N-diisopropyl-N-ethyl-amine, $c = 3 \cdot 10^{-6}$ mol/l): $\lambda_{max} = 589$ (+48), 545 (+26), 475 (−37), 430 (−53), 357 (+17), 318 (−17) nm ($\Delta\varepsilon$).

3a$^-$**/3b**$^-$. UV/Vis (ethanol + N,N-diisopropyl-N-ethyl-amine, $c = 3 \cdot 10^{-6}$ mol/l): $\lambda_{max} = 593$ (39820), 550 (19400), 511 (7500), 478 (19000), 388 (10000), 329 (25600) nm (ε); fluorescence (ethanol + N,N-diisopropyl-N-ethyl-amine, $c = 3 \cdot 10^{-6}$ mol/l): $\lambda_{em} = 600$ (1), 648 (0.3) nm (relative intensity), $\Phi_f = 0.19$.

3a′: CD (tetrahydrofuran + trifluoroacetic acid; c from $3 \cdot 10^{-3}$ to $3 \cdot 10^{-6}$ mol/l): $\lambda_{max} = 578$ (−47), 539 (−23), 457 (+43), 413 (+47), 357 (−14) nm ($\Delta\varepsilon$).

3b′: CD (tetrahydrofuran + trifluoroacetic acid; c from $3 \cdot 10^{-3}$ to $3 \cdot 10^{-6}$ mol/l): $\lambda_{max} = 578$ (+47), 539 (+23), 457 (−43), 413 (−47), 357 (+14) nm ($\Delta\varepsilon$).

3a′/3b′: UV/Vis (tetrahydrofuran + trifluoroacetic acid, $c = 3 \cdot 10^{-5}$ mol/l): $\lambda_{max} = 584$ (30000), 542 (15900), 507 (5600), 457 (16700), 432 (11700), 330 (13500) nm (ε); fluorescence (tetrahydrofuran + trifluoroacetic acid, $c = 3 \cdot 10^{-6}$ mol/l): $\lambda_{em} = 590$ (1), 634 (0.32) nm (relative intensity), $\Phi_f = 0.17$.

Acknowledgements

Critical comments from Doz. Dr. *K. Grubmayr* (Johannes Kepler Universität Linz), helpful advice with the calculations of chiroptical properties from Doz. Dr. *C. Scharnagl* (Univ. of Munich), and the kind permission of Dr. *M. A. Thompson* to download and use the ARGUS program are gratefully acknowledged. The calculations were performed at the supercomputing center of the ZID of the Johannes Kepler Universität Linz, which allocated the necessary CPU time.

References

[1] Etzlstorfer C, Falk H, Müller N, Schmitzberger W, Wagner UG (1993) Monatsh Chem **124**: 751
[2] Freeman D, Frolow F, Kapinus E, Lavie D, Meruelo D, Mazur Y (1994) J Chem Soc Chem Commun **1994**: 891
[3] Etzlstorfer C, Falk H, Mayr E, Schwarzinger S (1996) Monatsh Chem **127**: 1229
[4] Etzlstorfer C, Falk H (1993) Monatsh Chem **124**: 923
[5] Falk H, Meyer J (1994) Monatsh Chem **125**: 753
[6] Altmann R, Etzlstorfer C, Falk H (1997) Monatsh Chem **128**: 361
[7] Etzlstorfer C, Falk H, Müller N, Tran TNH (1996) Monatsh Chem **127**: 659
[8] Köhler M, Gafert J, Friedrich J, Falk H, Meyer J (1996) J Phys Chem **100**: 8567
[9] Hug W, Wagnière G (1972) Tetrahedron **28**: 1241
[10] MOPAC 6.0 DEC-3100 Ed (1990); Frank J, Seiler Res Lab, USAF Academy
[11] Ball and Stick 3.5: Müller N, Falk A (1993) Cherwell Scientific Publ Ltd, Oxford, UK
[12] Thompson MA (1992) ARGUS a quantum mechanical electronic structure program, version 1.1
[13] Tao N, Orlando M, Hyon JS, Gross M, Song PS (1993) J Am Chem Soc **115**: 2526; Falk H, Mayr E (1995) Monatsh Chem **126**: 1311
[14] Dai R, Yamazaki T, Yamazaki I, Song PS (1995) Biochim Biophys Acta **1231**: 58
[15] Ohrt JM, Parasarathy R (1969) Acta Cryst Suppl **1969**: 198

Received March 17, 1997. Accepted March 20, 1997